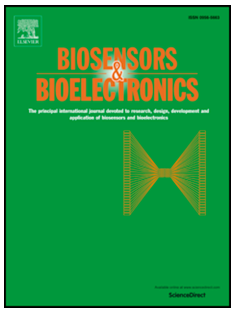

# Surface plasmon resonance imaging-based biosensor for multiplex and ultrasensitive detection of NSCLC-associated exosomal miRNAs using DNA programmed heterostructure of Au-on-Ag

Wenwen Wu, Xiaolin Yu, Jiangling Wu, Tao Wu, Yunpeng Fan, Wenqin Chen, Min Zhao, Haiping Wu, Xinmin Li, Shijia Ding

PII: S0956-5663(20)30821-6

DOI: https://doi.org/10.1016/j.bios.2020.112835

Reference: BIOS 112835

To appear in: *Biosensors and Bioelectronics*

Received Date: 6 September 2020

Revised Date: 28 October 2020

Accepted Date: 19 November 2020

Please cite this article as: Wu, W., Yu, X., Wu, J., Wu, T., Fan, Y., Chen, W., Zhao, M., Wu, H., Li, X., Ding, S., Surface plasmon resonance imaging-based biosensor for multiplex and ultrasensitive detection of NSCLC-associated exosomal miRNAs using DNA programmed heterostructure of Au-on-Ag, *Biosensors and Bioelectronics* (2020), doi: https://doi.org/10.1016/j.bios.2020.112835.

**CRediT authorship contribution statement**

**Wenwen Wu:** Conceptualization, Methodology, Software, Investigation, Data curation, Writing original draft, Project administration. **Xiaolin Yu:** Conceptualization, Methodology, Software, Investigation, Data curation, Writing-original draft, Project administration. **Jiangling Wu:** Software, Writing-original draft, Investigation. **Tao Wu:** Methodology, Formal analysis, Software. **Yunpeng Fan:** Software, Writing-original draft, Investigation. **Haiping Wu:** Methodology, Formal analysis, Software. **Wenqin Chen***:* Conceptualization, Data curation. **Min Zhao:** Resources, Software, Validation. **Xinmin Li:** Methodology, Formal analysis, Resources, Validation. **Shijia Ding:** Supervision, Methodology, Data curation, Funding acquisition, Project administration, Data curation.

# Surface plasmon resonance imaging-based biosensor for multiplex and ultrasensitive detection of NSCLC-associated exosomal miRNAs using DNA programmed heterostructure of Au-on-Ag

Wenwen Wu [a,1], Xiaolin Yu [b,1], Jiangling Wu [c], Tao Wu [b], Yunpeng Fan [a], Wenqin Chen [a], Min Zhao [a], Haiping Wu [a], Xinmin Li [a,*], Shijia Ding [a,*]

[a] *Key Laboratory of Clinical Laboratory Diagnostics (Ministry of Education), College of Laboratory Medicine, Chongqing Medical University, Chongqing 400016, China.*

[b] *Department of Laboratory Medicine, Zigong Fourth People's Hospital, Sichuan, 643000, China.*

[c] *Department of clinical laboratory, University-Town Hospital of Chongqing Medical University, Chongqing 401331, China.*



*** Corresponding author**

Tel: +86-23-68485688; Fax: +86-23-68485786.

E-mail: xinmnli@163.com (X. Li); dingshijia@cqmu.edu.cn, dingshijia@163.com (S. Ding)

**Author Contributions**

[1] W. Wu and X. Yu contributed equally to this work.

**ABSTRACT**

Exosomal miRNAs are potential tumor biomarkers for early diagnosis of non-small cell lung cancer (NSCLC). Herein, a surface plasmon resonance imaging (SPRi)-based biosensor was developed for simultaneous detection of multiplex NSCLC-associated exosomal miRNAs in a clinical sample using Au-on-Ag heterostructure and DNA tetrahedral framework (DTF). Exosomal miRNAs are captured by various DTF probes immobilized on the gold array chip. Subsequently, single-stranded DNA (ssDNA) functionalized silver nanocube (AgNC) hybridizes with the captured exosomal miRNAs and then the ssDNA-coated Au nanoparticles assembled on the surface of AgNC, forming Au-on-Ag heterostructures as essential labels to realize amplified SPR response. With the aid of DNA programmed Au-on-Ag heterostructure and DTF, the SPRi-based biosensor exhibits wide detection range from 2 fM to 20 nM, ultralow limit of detection of 1.68 fM, enhanced capture efficiency, and improved antifouling capability. Furthermore, the biosensor enables accurate discrimination of NSCLC patients based on detection results of exosomal miRNAs. Overall, this developed biosensor is a promising tool for multiplex exosomal miRNAs detection, providing a new possibility for early diagnosis of NSCLC.

**Key words:** Non-small cell lung cancer; Surface plasmon resonance imaging; Exosomal miRNAs; Metal heterostructure; Multiplex detection.

## 1. Introduction

Lung cancer is leading cause of cancer-related deaths (Bray et al., 2018). Non-small cell lung cancer (NSCLC), the most common type of lung cancer, are always diagnosed at advanced stages due to the lack of typical clinical symptoms, leading to ultralow five-year survival rate of 15% (Pao and Girard, 2011; Siegel et al., 2017). Early diagnosis can prominently improve survival rate and decrease cost of treatment (Rabinowits et al., 2009). However, routine diagnostic methods based on proteomic biomarkers, in vivo imaging, and tissue biopsy are limited owing to low detection throughput, poor diagnosis accuracy, and severe sampling invasiveness. Therefore, the early diagnosis of NSCLC with accurate and noninvasive is still an urgent requirement.

Exosomes are small nanovesicles ranging from 30 to 150 nm and secreted into bodily fluids by alive cells (Zomer et al., 2010). They can tightly participate in cell-to-cell communication through transferring enclosed biomolecules, including DNA, RNA, and proteins (Mathieu et al., 2019; Shen et al., 2018). Among them, exosomal miRNAs, a kind of noncoding and endogenous small RNAs (20-24 bp) that mediates protein level by suppressing the expression of target mRNAs, not only account for strong percentage in total exosomal RNA, but also play essential roles in tumor progression and metastasis (Cho et al., 2019; Jiang et al., 2017). Studies have demonstrated that exosomal miRNAs (miRNA-21, miRNA-378, miRNA-200, and miRNA-139) are potential biomarkers for screening of NSCLC (Cazzoli et al., 2013). What's more, exosomal miRNAs are endowed with two considerable traits compared to serum miRNAs, which also contribute to improve the diagnosis of NSCLC. The one is that the concentration of exosomes derived from tumor cells has obviously greater than that of exosomes derived from normal cells (Heneghan et al., 2010). The other is that the exosomal membrane protects encapsulated miRNAs from being degraded by RNase (Liu et al., 2019). Thus, detection of exosomal miRNAs holds great promise for noninvasive and credible diagnosis of NSCLC.

Quantitative reverse transcription polymerase chain reaction (qRT-PCR) is a leading method for miRNAs analysis (Tavallaie et al., 2018). However, the method

has been exposed some defects (toilsome primer design and false positive error), because of intrinsic properties of miRNAs, including short length, low abundance, and high sequence similarity (Lee et al., 2019). Accordingly, many attempts have been performed to develop alternative methods for the detection of exosomal miRNAs (Ma et al., 2018; Xia et al., 2018). Nevertheless, these methods encountered toilsome labeling of signal molecules, such as fluorophores, methylene blue, and ferrocene. What's worse, it is difficult to reach accurate conclusion from the result of single exosomal miRNA analysis due to the correlation of a biomarker with more than one cancer. To improve the accuracy of the early diagnosis of NSCLC, it is highly desired to develop methods capable of simultaneously detecting multiple exosomal miRNAs in a single clinical sample.

Surface plasmon resonance imaging (SPRi)-based biosensor is a high-throughput, label-free technique that can detect various analytes of clinical interest in real time, visible, and noninvasive fashion (Al Mubarak et al., 2020; Wang, Q. et al., 2019). Compared to other sensing methods (surface-enhanced Raman scattering, fluorescence, and electrochemistry), SPRi-based biosensor does not require extra dyes, tags, or special reagents to product output signal (Thakur et al., 2020; Wang, Q. et al., 2019; Wang, X. et al., 2019). Given these advantages, the biosensor is an optimal sensing platform for simultaneous detection of multiple exosomal miRNAs. However, it is still challenging to detect traces of exosomal miRNAs using SPRi-based biosensor owing to the lack of effective SPR amplifier. On the other hand, the nonspecific adsorption of complex physiological matrices (proteins, nucleic acids, and lipids) on sensor chip can conceal specific signal, leading to drastic reduction in assay specificity and sensitivity, which severely precludes its clinical applications (Jiang et al., 2020).

Plasmonic metal nanostructures, especially gold (Au) and silver (Ag), have given rise to considerable attention as labels for SPR signal enhancement because of their tunable optical property and simple synthesis (Mahmoudpour et al., 2019; Zhang et al., 2018). However, single type of metal nanostructure is limited in improving sensitivity. An effective method to address the issue is to introduce heterogeneous nanostructures

with diverse metal components (Lambert et al., 2018; Liu et al., 2017). To simply and directly assemble heterostructures, DNA molecules can act as promising linkers owing to the programmability and binding accuracy of base pair (Laramy et al., 2019; Li et al., 2019). Based on the hybridization between single-stranded DNA (ssDNA) and complementary sequences attached to the surfaces of metal nanostructures, different configurations of metal heterostructures have been created, exhibiting excellent synergistic effects (Ji et al., 2019; Zhao and Xu, 2020). In this regard, DNA-mediated metal heterostructures provide new opportunities in the construction of ideal amplifier for the enhancement of SPR signal.

Herein, a SPRi-based biosensor was developed for ultrasensitive detection of NSCLC-associated exosomal miRNAs by synergizing between Au-on-Ag heterostructure and DNA tetrahedral framework (DTF). DTF, a kind of emerging DNA nanomaterial with prominent mechanical rigidity and structural stability (Pei et al., 2010; Xu et al., 2020), not only improves the binding efficiency of probes through reducing their entanglement and overcrowding effect, but enhances the antifouling ability of the sensor interface (Liu et al., 2020; Nie et al., 2018; Zhang et al., 2020). Exosomal miRNAs bound specifically to DTF probes tethered on a gold array chip, initiating the self-assembly of Au-on-Ag heterostructures to arouse great SPR response signal for ultrasensitive detection of exosomal miRNAs. This high-throughput biosensor provides an accurate platform for early diagnosis of NSCLC.

## 2. Experimental Section

### *2.1. Materials and Chemicals*

Silver trifluoroacetate ($CF_3COOAg$), sodium hydrosulfide hydrate (NaSH), ethylene glycol (EG), poly (vinyl pyrrolidone) (PVP, MW ≈ 55000), and 6-Mercapto-1-hexanol (MCH) were purchased from Sigma-Aldrich Chemical Co., Ltd (St. Louis, MO, U.S.A.). Bovine serum albumin (BSA) was obtained from Thermo Fisher Scientific Co., Ltd (Wilmington, USA). $HAuCl_4 \cdot 4H_2O$ was purchased from Sinopharm Chem Co., Ltd (Shanghai, China). All HPLC-purified oligonucleotide sequences (displayed in Table S1), tris (2-carboxyethyl) phosphine

(TCEP), diethylpyrocarbonate (DEPC), and triton X-100 were obtained from Sangon Biotechnology Co. Ltd (Shanghai, China). Aqueous solutions were prepared with ultrapure water (Millipore, MA). All other reagents were of analytical grade. The oligonucleotides of DTF probes were dissolved in TM buffer (20 mM Tris, 50 mM $MgCl_2$, pH 8.0), and the rest were dissolved in TE buffer (10 mM Tris-HCl, 1 mM EDTA, pH 8.0). All solutions were treated with 1% DEPC to prevent the effects of RNase.

*2.2. Apparatus and Measurements*

A home-built SPRi platform was used to analyze exosomal miRNAs. The SPRi platform, comprising of a laser source for SPR excitation, a sensor chip, and a CCD camera for image acquisition, was capable of simultaneously detecting multiplex targets with two separate channels and gold array chips. Red-emitting diode (LED, 650 nm) was used as an optical source. P-polarization of the light was obtained with a sheet polarizer, and the matching liquid (n ¼ 1.616) was mediated between the sensor chip and prism. The image reflected through the prism was captured by a 12-bit CCD camera (Retiga 1300 from QImaging). All sensorgrams were analyzed by a lab-developed program written in LabVIEW. The sensorgram displayed a time course of resonance units (RU). The RU was defined as the SPR angle, where 1000 RU equaled to about 0.1° in angle change. The SPR angle change was proportional to changes in the mass on the sensor surface. The SPRi biosensor detected the shift in the SPR angle by measuring the intensity change in the reflected light at a fixed incident angle. ssDNA functionalized AgNC and AuNP were characterized by UV–vis absorption spectra Nano-Drop1000 (Thermo, USA).

*2.3. Preparation of DTF probes*

DTFs were synthesized based on base pairing referring to the previous work with little modification (Lin et al., 2016). Firstly, DNA strands were dissolved with TM buffer containing 30 mM TCEP to reduce the crosslinking of thiol groups. Subsequently, the equal concentration of four DNA strands (12 μM) were mixed and heated at 95 □ for 5 min, closely followed by 4 □ for 1 min to form the DTFs. Then, the synthesized DTFs were kept at 4 □ for future use.

*2.4. Preparation of ssDNA-functionalized AuNPs*

AuNPs and ssDNA-functionalized AuNPs were prepared according to the previous literature with little adjustment (Liu and Lu, 2006). In short, sodium citrate (10.1 mL, 34 mM) was added rapidly to the boiling solution of $HAuCl_4$ (88.2 mL, 1 mM). After the color changed from pale yellow to wine-red, the mixture was stopped heating and cooled to room temperature (RT) with continued stirring. The products were stored at 4 °C for further use. ssDNA (L1-L8)-functionalized AuNPs were prepared as follows. Firstly, 49 μL thiolated ssDNA (100 μM), 5 μL acetate (500 mM, pH 5.2), and 0.15 μL TCEP (100 mM) were mixed at RT for 1 h. Then the mixture was added into 1.6 mL AuNP solution, and the resultant solution was stored in a drawer at RT for at least 16 h. After 16 μL Tris-acetate (500 mM, pH 8.2) was added to the mixture, 160 μL NaCl (1 M) was added dropwise to the mixture every four hours (25, 35, 45, 55 μL were added respectively). Subsequently, the resulting mixture was stored in a drawer overnight. Lastly, the mixture was centrifuged (10 000 rpm, 10 min) to remove the excess reagents, and the red precipitate was washed and dispersed in 1 × PBS for further use.

*2.5. Preparation of ssDNA-functionalized AgNCs*

Firstly, AgNCs were synthesized according to the previous report (Wang et al., 2013). Briefly, 5 mL of ethylene glycol (EG) was heated to 150 °C in an oil bath under magnetic stirring, and then NaHS (0.06 mL, 3 mM) was quickly injected. After 2 min, HCl (0.5 mL, 3 mM in EG) was injected into the heated solution, followed by the addition of PVP (1.25 mL, 20 mg $mL^{-1}$ in EG). After another 2 min, $CF_3COOAg$ (0.4 mL, 282 mM in EG) was also added into the mixture. The AgNCs were obtained by quenching the reaction with an ice-water bath after 60 min. After centrifugation (6 000 rpm, 10 min) and washing by acetone and ultrapure water three times, the products were dispersed and stored in ultrapure water. ssDNA (L1, L3, L5, and L7)-functionalized AgNCs were prepared by incubating a mixture, consisting of thiolated ssDNA (10 μL, 10 μM), freshly prepared AgNCs (100 μL), and ultrapure water (200 μL), at 4 □ with constantly shake for 12 h. Then the products were centrifuged (6 000 rpm, 5 min) and dispersed in 1 × PBS for further use.

*2.6. Probes immobilization on the gold array chip*

Before the immobilization of thiolated DTFs or ssDNA (C1) capture probes, the surface of the gold array chip was treated with the fresh piranha solution (70% $H_2SO_4$, 30% $H_2O_2$) for 10 min to eliminate the adsorbed impurities, then rinsed thoroughly with ultrapure water, and finally dried the chip with nitrogen. Afterwards, the capture probes (40 μL, 1 μM) were added onto the chip and incubated at 4 □ overnight. These probes could be assembled onto the gold chip by Au-S chemistry. Then, BSA (1%) and MCH (1%) were incubated with the chip for 1 h and 30 min, respectively. It is worth nothing that DTFs functionalized chip was not been blocked by BSA and MCH. After washing with ultrapure water and drying with nitrogen, the chip was docked into the SPRi instrument for further use.

*2.7. SPRi measurement*

First, PBS (0.01 M) was injected into the instrument at the speed of 8 μL $min^{-1}$. After the instrument reached a steady state, the targets were injected at a speed of 50 μL $min^{-1}$. After 2 min 40 s, the injection speed was slowed down to 5 μL $min^{-1}$ to sure the enough hybridization time of the targets and DTFs. When the SPR signal stabled again, the ssDNA-functionalized AgNC were injected into the flow cell for hybridizing with the captured targets. After which, two kinds of ssDNA-functionalized AuNPs were successively injected into the flow cell at the same rate to form the heterostructure of Au-on-Ag. After the Au-on-Ag is completely passed, PBS was injected again at a speed of 5 μL $min^{-1}$ to rinse the chip and check the binding affinity.

*2.8. Isolation of exosomes and exosomal miRNAs*

The operation of exosome isolation was as follows. First, human plasma was centrifuged (10 000 × g, 30 min) twice to remove cell debris, intact cells, and large microvesicles, then the supernatant was collected and ultracentrifuged (100 000 × g, 70 min) to isolate exosomes. After pouring off the supernatant, the isolated exosomes were dispersed in a large volume of PBS, filtered by 0.22 μm filters, and ultracentrifuged (100 000 × g, 70 min) to eliminate protein impurity. After discarding the supernatant, these nanoscale vesicles were resuspended in 100 μL PBS and stored

at -80 □ prior to use. In this part, all centrifugation and sample processing were carried out at 4 □. Total RNA was extracted from the exosome by Trizol (Lasser, 2013).

## 3. Results and discussion

### *3.1. Design principle of the biosensor*

Taking one of exosomal miRNAs for example, the principle of this biosensor was adequately illustrated in Scheme 1. As shown in Scheme 1A, DTF was assembled by the hybridization of four strands (S1-S4). The unconfined sequence in DTF was used to capture exosomal miRNA. AgNC was synthesized step by step and then functionalized with thiolated ssDNA (L1), resulting in the formation of L1@AgNC. The L1 was used to hybridize with the captured target (Scheme 1B). As depicted in Scheme 1C, a part of the target specifically bound to the DTFs immobilized on the SPRi chip. Subsequently, L1@AgNC complex combined with the other part of the target to construct a sandwich structure. Finally, L2@AuNP and L1@AuNP were consecutively assembled on the surface of the AgNC through the hybridization of strands, forming Au-on-Ag heterostructure and achieving effective signal amplification for sensing target. By incubating different DTFs on the four detection sites of the SPRi chip, multiple and simultaneous analysis of exosomal miRNAs was achieved (Scheme 1D).

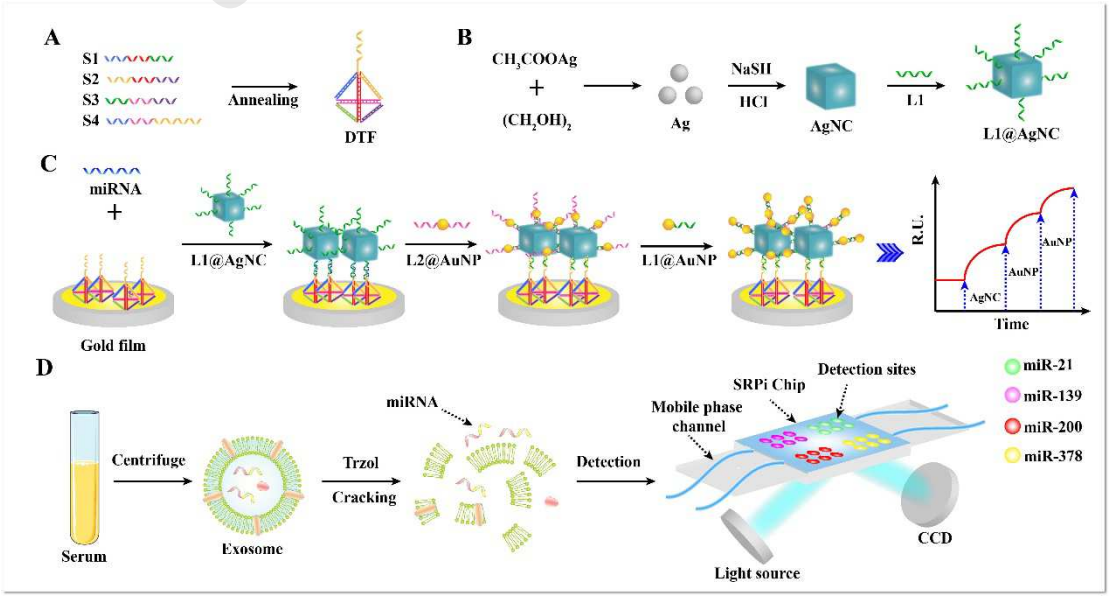


**Scheme 1**. Schematic illustration of the multiplex exosomal miRNAs detection using

SPRi biosensor. (A) Self-assembly of DTF, (B) Synthesis of ssDNA-functionalized AgNC, (C) Self-assembly of Au-on-Ag heterostructures on the SPRi chip, (D) Extraction and detection of exosomal miRNAs.

*3.2. Feasible analysis of the biosensing strategy*

To verify successful assembly of DTFs, the size and shape of the synthesized DTFs were characterized by 3% agarose gel electrophoresis and atomic force microscopy (AFM), respectively. As depicted in Fig. 1A, DTFs (lane 5) moved more slowly than single strand (lane 1) and the other combinations of two and three fragments (lane 2, 3, 4). AFM image showed many small triangles, which is in accordance with the face of DTF (Fig. 1B). These results indicated the successful synthesis of DTFs. Then, the feasibility of the developed biosensor for miRNA detection was further evaluated. As shown in Fig. 1C, in the presence of target miRNA, the SPR signal gradually enhanced with the addition of L1@AgNC, L2@AuNP, and L1@AuNP (curve a), suggesting that AuNPs were tethered to the surface of AgNC, successfully forming Au-on-Ag heterostructure. In contrast, a negligible SPR response change was observed (curve b), because neither L1@AgNC nor ssDNA-coated AuNPs could bind to the surface of the sensor chip in the absence of the miRNA, indicating that these metal nanostructures generated negligible non-specific adsorption on the DTFs-gold chip. In addition, the difference in response signal could be directly observed by the brightness of SPRi image. These results demonstrated that the developed biosensor had good feasibility for exosomal miRNAs analysis.

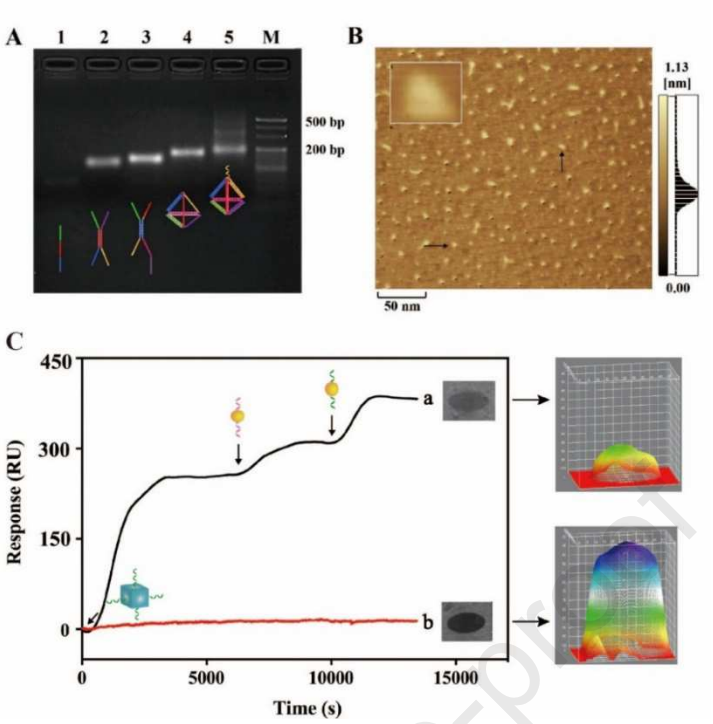


**Fig. 1** Evaluation the feasibility of the biosensor. (A) Characterization of DTFs with 3% gel electrophoresis: (1) S1, (2) S3 + S4, (3) S1 + S2, (4) S1 + S2 + S3, (5) S1 + S2 + S3 + S4, and (M) 20 bp DNA marker. The concentrations of all DNA strands were 1.0 μM. (B) AFM image of DTFs, scale bar is 50 nm. (C) Typical SPR sensorgrams responding to (a) 20 nM target and (b) blank control. The intensity analysis of 3D SPRi image was presented in the right of the sensorgram.

*3.3. Evaluation of Au-on-Ag heterostructure and antifouling capacity of the biosensor*

To demonstrate the superiority of Au-on-Ag heterostructure, comparison with AuNPs and AgNCs was performed. Firstly, the morphologies of AuNP and AgNC were characterized by TEM image, respectively. As shown in Fig. S1A and C, these nanostructures showed good uniformity and dispersion, suggesting the successful synthesis of AuNPs and AgNCs. In addition, ssDNA-coated AuNPs and ssDNA-functionalized AgNCs exhibited characteristic DNA absorption peak at 260 nm compared to AuNPs and AgNCs (Fig. S1B and D), demonstrating that ssDNA was bound to the surface of metal nanostructure. As shown in Fig. 2A, the SPR response signals produced by different metal nanostructures followed the order of Au-on-Ag > AgNCs > AuNPs. Responding to the same concentration of target (20 nM), Au-on-Ag heterostructure had about 6.0 times higher SPR response signal than AuNPs and 1.6

times higher signal than AgNCs. The high signal of Au-on-Ag was attributed to the unique nanostructure and the synergy between AgNCs and AuNPs.

To evaluate the antifouling capacity of the SPR biosensor, ssDNA (C1)-modified chip and DTFs-modified chip were compared in 10% diluted plasma. The C1 had the same DNA sequence as the free end of DTFs. As shown in Fig. 3B, the biosensor docked into C1-modified chip showed high background noise (blue bar), which originated from the nonspecific adsorption of complex biomolecules in plasma and metal nanostructures. Even though the addition of target into this system, the increased SPR signal was negligible (red bar). These results indicated that ssDNA-modified chip failed to operate in serum samples. However, the biosensor docked into DTFs-modified chip displayed low background noise (blue bar), demonstrating a strong resistance to nonspecific adsorption. The obviously improved SPR response signal was observed in the presence of the same concentration of target (20 nM) compared to C1-modified chip, suggesting that DTFs could improve hybridization efficiency between targets and probes. These results indicated that DTFs-modified chip allows the biosensor to normally function in clinical samples.

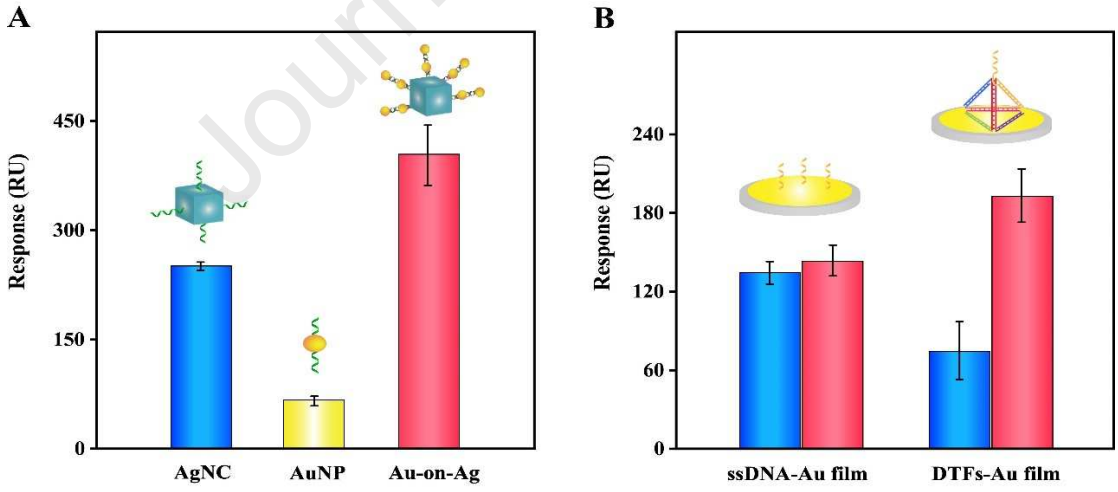


**Fig. 2** (A) Comparison of SPR signal produced by AgNC, AuNP, and Au-on-Ag heterostructures. (B) Evaluation of antifouling capacity of the biosensor in 10% diluted plasma. The red bar stands for SPR signal responding to 20 nM target, and the blue bar stands for background noise. All data expressed as mean ± standard variation (n = 3).

*3.4. Evaluation of the sensitivity of the biosensor*

To obtain the highest sensitivity of the proposed biosensor, some experimental conditions were investigated, including the layers of AuNPs on AgNCs and the concentration of DTFs. As depicted in Fig. 3A, with the increase of AuNP layers, the SPR signal gradually improved and reached peak at two layers of AuNPs. In addition, the concentration of DTFs was also a key factor for SPR signal. As shown in Fig. 3B, the SPR signal grew with the growing concentration of DTFs from 1 μM to 3 μM and then declined rapidly with higher concentration of DTFs. The reason to the decrease of response signal is that an excess of DTFs can cover up the capture probes lied in DTFs. Thus, 3 μM was selected as the optimal concentration of DTFs. Under optimal experiment conditions, the sensitivity of the proposed biosensor was tested. As shown in Fig. 3C, SPR signal increased with the increase of target concentration ranging from 2 fM to 20 nM. In this range, a favorable linear relationship between SPR signal and the logarithmic value of miRNA-21 concentration was exhibited (Fig. 3D). However, compared to 2 fM and 20 nM target, the SPR signal showed subtle shift responding to 0. 2 fM and 200 nM target. The regression equation was $y = 42.887 \times \lg c$ (fM) - 9.722 ($R^2 = 0.9810$), where y was the SPR response signal and *c* was the concentration of target miRNA. Also, the limit of detection (LOD) was calculated to be 1.68 fM based on a 3σb/slope, the σb stands for the standard deviation of three blank samples. Furthermore, linear relationships between SPR signal and the logarithmic value of miRNA-378, miRNA-139, and miRNA-200 concentration were evaluated, and the results were shown in Fig. S3. In addition, to highlight the signal amplification of the AuNPs, the sensitivity of the biosensor based on AgNCs was investigated. As shown in Fig. S4, the LOD was calculated to be 2.74 fM, indicating that AuNPs contributed to improving the sensitivity of this biosensor. Compared with other SPR and SPRi biosensor for exosomal miRNA detection, the proposed strategy achieved a superior sensitivity and wider linear range (Table S2), owing to the powerful SPR response of Au-on-Ag heterostructure and antifouling ability. In addition, compared to the reported multiplex detection systems that usually needed to label many different fluorophores (Lee et al., 2016; Wang et al., 2020), the developed biosensor revealed lower LOD without marking any signal molecules.

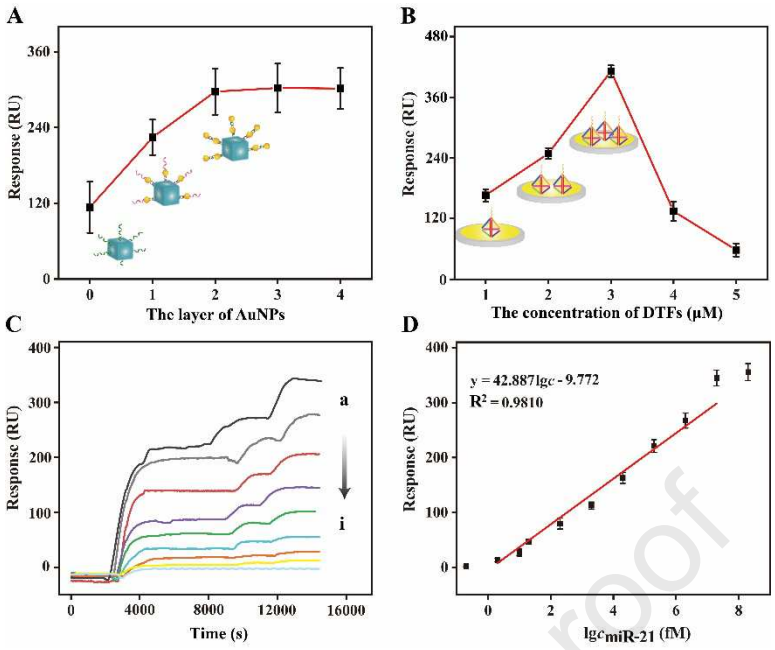


335

336 **Fig. 3** Optimization of experimental parameters: (A) The layers of AuNPs on AgNCs
337 (B) and the concentration of DTFs. Evaluation of the sensitivity of the biosensor: (C)
338 SPR sensorgrams responding to $2 \times 10^7$, $2 \times 10^6$, $2 \times 10^5$, $2 \times 10^4$, $2 \times 10^3$, 200, 20, 10,
339 2 fM exosomal miRNA-21 (from a to i) and (D) the corresponding linear relationship
340 between SPR signal and logarithmic value of miRNA concentrations. Error bar
341 represents the standard deviation (n = 3).

342 *3.5. Multiplex detection of the biosensor*

343 To verify the high throughput of the SPRi biosensor, we immobilized different
344 DTFs on four detection sites of one gold array chip, including DTF-21, DTF-378,
345 DTF-200, and DTF-139 that are employed for sensing miRNA-21, miRNA-378,
346 miRNA-200, and miRNA-139, respectively. As shown in Fig. 4, Under optimal
347 experiment conditions, upon miRNA-21, miRNA-378, miRNA-200, and miRNA-139
348 were added into the system, respectively. After adding Au-on-Ag heterostructures,
349 distinct SPR response signals were observed in the corresponding detection site,
350 indicting one target bound only to one probe. In presence of four miRNAs, all four
351 detection sites showed outstanding SPR signals, suggesting that this biosensor was
352 able to simultaneously detect four miRNAs. In addition, the response signals

generated by four miRNAs could be visually observed by the SPR image and 3D surface plot (Fig. S6). These results demonstrated that the SPRi biosensor possessed high throughput and good specificity.

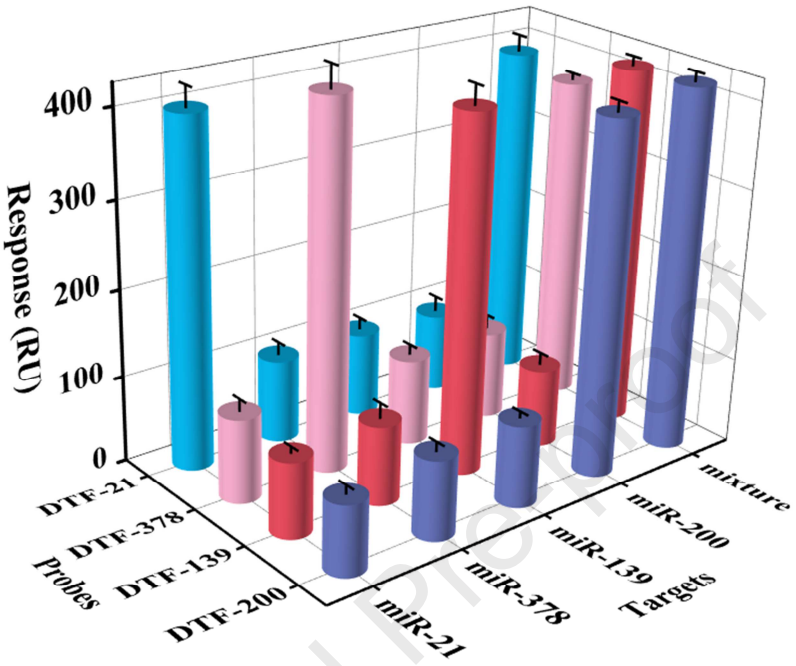


**Fig. 4** Multiplex and selective analysis of miRNAs. The abscissa refers to DTFs incubated in different areas on gold chip, the ordinate refers to the different miRNAs injected into the SPRi system. The concentrations of DTF were 3 μM, and miRNAs were 20 nM. Error bar represents the standard deviation (n = 3).

*3.6. Detection of exosomal miRNAs in clinical samples*

To evaluate the applicability of the biosensor for the diagnosis of NSCLC, four miRNAs derived from exosomes in clinical samples were tested. Firstly, 10 clinical specimens (5 healthy volunteers and 5 patients) were collected from a local hospital. The purified exosomes were analyzed by TEM and nanoparticle tracking analysis. As shown in Fig. S2, the extracted exosomes had a typical cup shape, and its diameter was about 90 nm, which were consistent with previously reported characteristics (Tang et al., 2017). Then, we extracted miRNA from exosomes and measured the expression levels of them using our developed biosensor. As shown in Fig. 5, the enhanced SPR response signals for patients' miRNAs were observed (baby blue bar).

Compared to the healthy people (H1-H5), four exosomal miRNAs in NSCLC patients (P1-P5) had significant over-expression. The NSCLC samples could be well discriminated from the healthy ones ($P < 0.05$), which demonstrated that this biosensor was a promising method for sensitive and multiplex biomarkers detection toward NSCLC diagnosis. However, it was hard to diagnose NSCLC by the detection of exosomal miRNA-21, owing to the association of exosomal miRNA-21 with colon adenocarcinoma, breast cancer, and lung cancer (Lee et al., 2019; Wang et al., 2020). Therefore, detection of multiplex miRNA has more clinic value than single miRNA.

In addition, to demonstrate the credibility of the developed biosensor, the comparison between qRT-PCR and the biosensor was performed. As shown in Fig. S5, the relative expression levels of exosomal miRNA-21 detected by qRT-PCR were highly consistent with the results of the developed SPRi biosensor. These results demonstrated that the developed SPRi biosensor was credible to detect exosomal miRNA in clinical samples.

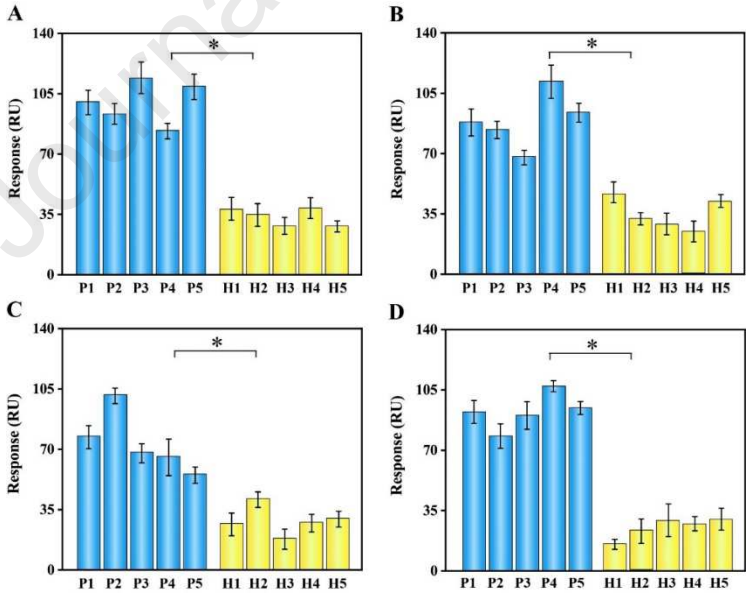


**Fig. 5** Using this proposed method to detect (A) exosomal miRNA-21, (B) exosomal miRNA-378, (C) exosomal miRNA-200, (D) exosomal miRNA-378 derived from clinical samples. Error bar represents the standard deviation (n = 3).

## 4. Conclusion

In summary, we successfully constructed a novel SPRi biosensor for ultrasensitive detection of multiplex exosomal miRNAs based on Au-on-Ag heterostructure and DTF. Compared with other biosensors reported previously, the SPRi biosensor exhibits several distinctive merits for exosomal miRNAs analysis. First, the immobilization of DTF on the gold array chip reduces nonspecific adsorption, which allows the developed biosensor to operate well in complex biological fluid. Second, benefiting from the outstanding SPR response capability of DNA programmed Au-on-Ag heterostructure, this biosensor exhibited excellent sensitivity down to 1.68 fM and wide dynamic range. Third, the developed biosensor possesses high-throughput capability that can simultaneously detect four exosomal miRNAs in a single clinical sample. Most importantly, based on the differences of exosomal miRNAs expression, the biosensor can precisely identify NSCLC patients with noninvasive way. Considering these advantages (robust antifouling capability, ultrahigh sensitivity, and high detection throughput), this SPRi-based biosensor provides a new platform for the early diagnosis of NSCLC and has great application potential in clinical diagnosis field.

## Declaration of competing interest

The authors declare no competing interests.

## Acknowledgment

This work was funded by the financial support from the Natural Science Foundation of China (81873980, 21804015), the National Science and Technology Major Project of the Ministry of Science and Technology of China (2018ZX10732202), the Science and Technology Project of the Health Planning Committee of Sichuan (19PJ159), and the Natural Science Foundation Project of Chongqing (cstc2018jcyjAX0251).

## References

Al Mubarak, Z.H., Premaratne, G., Dharmaratne, A., Mohammadparast, F., Andiappan, M., Krishnan, S., 2020. Lab Chip 20(4), 717-721.

419 Bray, F., Ferlay, J., Soerjomataram, I., Siegel, R.L., Torre, L.A., Jemal, A., 2018. CA
420 Cancer J. Clin. 68(6), 394-424.
421 Cazzoli, R., Buttitta, F., Di Nicola, M., Malatesta, S., Marchetti, A., Rom, W.N., Pass,
422 H.I., 2013. J Thorac Oncol. 8(9), 1156-1162.
423 Cho, S., Yang, H.C., Rhee, W.J., 2019. Biosens. Bioelectron. 146, 111749.
424 Heneghan, H.M., Miller, N., Kelly, R., Newell, J., Kerin, M.J., 2010. Oncologist 15(7),
425 673-682.
426 Ji, M., Ma, N., Tian, Y., 2019. Small 15(26), e1805401.
427 Jiang, C., Wang, G., Hein, R., Liu, N., Luo, X., Davis, J.J., 2020. Chem. Rev. 120(8),
428 3852-3889.
429 Jiang, Y., Shi, M., Liu, Y., Wan, S., Cui, C., Zhang, L., Tan, W., 2017. Angew. Chem.
430 Int. Ed. 56(39), 11916-11920.
431 Lambert, A., Yang, Z., Cheng, W., Lu, Z., Liu, Y., Cheng, Q., 2018. ACS Sens. 3(9),
432 1639-1646.
433 Laramy, C.R., O'Brien, M.N., Mirkin, C.A., 2019. Nat. Rev. Mater. 4(3), 201-224.
434 Lasser, C., 2013. Methods Mol. Biol. 1024, 109-128.
435 Lee, J.H., Kim, J.A., Jeong, S., Rhee, W.J., 2016. Biosens. Bioelectron. 86, 202-210.
436 Lee, J.U., Kim, W.H., Lee, H.S., Park, K.H., Sim, S.J., 2019. Small 15(17), e1804968.
437 Li, N., Shang, Y., Xu, R., Jiang, Q., Liu, J., Wang, L., Cheng, Z., Ding, B., 2019. J.
438 Am. Chem. Soc. 141(45), 17968-17972.
439 Lin, M., Song, P., Zhou, G., Zuo, X., Aldalbahi, A., Lou, X., Shi, J., Fan, C., 2016.
440 Nat Protoc. 11(7), 1244-1263.
441 Liu, J., Lu, Y., 2006. Nat Protoc. 1(1), 246-252.
442 Liu, L., Lu, H., Shi, R., Peng, X.X., Xiang, Q., Wang, B., Wan, Q.Q., Sun, Y., Yang, F.,
443 Zhang, G.J., 2019. Anal. Chem. 91(20), 13198-13205.
444 Liu, R., Wang, Q., Li, Q., Yang, X., Wang, K., Nie, W., 2017. Biosens. Bioelectron. 87,
445 433-438.
446 Liu, Z., Lei, S., Zou, L., Li, G., Xu, L., Ye, B., 2020. Biosens. Bioelectron. 147,
447 111759.
448 Ma, D., Huang, C., Zheng, J., Tang, J., Li, J., Yang, J., Yang, R., 2018. Biosens.

Bioelectron. 101, 167-173.

Mahmoudpour, M., Ezzati Nazhad Dolatabadi, J., Torbati, M., Pirpour Tazehkand, A., Homayouni-Rad, A., de la Guardia, M., 2019. Biosens. Bioelectron. 143.

Mathieu, M., Martin-Jaular, L., Lavieu, G., Thery, C., 2019. Nat. Cell Biol. 21(1), 9-17.

Nie, W., Wang, Q., Zou, L., Zheng, Y., Liu, X., Yang, X., Wang, K., 2018. Anal. Chem. 90(21), 12584-12591.

Pao, W., Girard, N., 2011. Lancet Oncol. 12(2), 175-180.

Pei, H., Lu, N., Wen, Y., Song, S., Liu, Y., Yan, H., Fan, C., 2010. Adv. Mater. 22(42), 4754-4758.

Rabinowits, G., Gercel-Taylor, C., Day, J.M., Taylor, D.D., Kloecker, G.H., 2009. Clin. Lung Cancer 10(1), 42-46.

Shen, W., Guo, K., Adkins, G.B., Jiang, Q., Liu, Y., Sedano, S., Duan, Y., Yan, W., Wang, S.E., Bergersen, K., Worth, D., Wilson, E.H., Zhong, W., 2018. Angew. Chem. Int. Ed. 57(48), 15675-15680.

Siegel, R.L., Miller, K.D., Fedewa, S.A., Ahnen, D.J., Meester, R.G.S., Barzi, A., Jemal, A., 2017. CA Cancer J. Clin. 67(3), 177-193.

Tang, Y.T., Huang, Y.Y., Zheng, L., Qin, S.H., Xu, X.P., An, T.X., Xu, Y., Wu, Y.S., Hu, X.M., Ping, B.H., Wang, Q., 2017. Int. J. Mol. Med. 40(3), 834-844.

Tavallaie, R., McCarroll, J., Le Grand, M., Ariotti, N., Schuhmann, W., Bakker, E., Tilley, R.D., Hibbert, D.B., Kavallaris, M., Gooding, J.J., 2018. Nat. Nanotechnol. 13(11), 1066-1071.

Thakur, A., Qiu, G., Xu, C., Han, X., Yang, T., Ng, S.P., Chan, K.W.Y., Wu, C.M.L., Lee, Y., 2020. Sci. Adv. 6(26), eaaz6119-eaaz6119.

Wang, H., He, D., Wan, K., Sheng, X., Cheng, H., Huang, J., Zhou, X., He, X., Wang, K., 2020. Analyst 145(9), 3289-3296.

Wang, Q., Zou, L., Yang, X., Liu, X., Nie, W., Zheng, Y., Cheng, Q., Wang, K., 2019. Biosens. Bioelectron. 135, 129-136.

Wang, X., Hou, T., Lin, H., Lv, W., Li, H., Li, F., 2019. Biosens. Bioelectron. 137, 82-87.

Wang, Y., Zheng, Y., Huang, C.Z., Xia, Y., 2013. J. Am. Chem. Soc. 135(5), 1941-1951.

Xia, Y., Wang, L., Li, J., Chen, X., Lan, J., Yan, A., Lei, Y., Yang, S., Yang, H., Chen, J., 2018. Anal. Chem. 90(15), 8969-8976.

Xu, S., Chang, Y., Wu, Z., Li, Y., Yuan, R., Chai, Y., 2020. Biosens. Bioelectron. 149, 111848.

Zhang, J., Lin, B., Wu, L., Huang, M., Li, X., Zhang, H., Song, J., Wang, W., Zhao, G., Song, Y., Yang, C., 2020. Angew. Chem. Int. Ed. 59(33), 14115-14119.

Zhang, Y., Shuai, Z., Zhou, H., Luo, Z., Liu, B., Zhang, Y., Zhang, L., Chen, S., Chao, J., Weng, L., Fan, Q., Fan, C., Huang, W., Wang, L., 2018. J. Am. Chem. Soc. 140(11), 3988-3993.

Zhao, Y., Xu, C., 2020. Adv. Mater., e1907880.

Zomer, A., Vendrig, T., Hopmans, E.S., van Eijndhoven, M., Middeldorp, J.M., Pegtel, D.M., 2010. Commun. Integr. Biol. 3(5), 447-450.

# Highlights

- DNA programmed heterostructure of Au-on-Ag endowed the SPRi biosensor with ultrahigh sensitivity.
- The high-throughput biosensor was capable of simultaneously detecting four exosomal miRNAs in a clinical sample.
- The biosensor showed enhanced antifouling capability, benefiting from DTF.
- The biosensor could accurately diagnose NSCLC patients from the healthy ones.

## Declaration of Interest Statement

We declare that we have no financial and personal relationships with other people or organizations that can inappropriately influence our work, there is no professional or other personal interest of any nature or kind in any product, service and/or company that could be construed as influencing the position presented in, or the review of, the manuscript entitled "**Surface plasmon resonance imaging-based biosensor for multiplex and ultrasensitive detection of NSCLC-associated exosomal miRNAs using DNA programmed heterostructure of Au-on-Ag**".